

Stationkeeping of a Flux-Pinned Satellite Network

Michael C. Norman¹
Cornell University, Ithaca, NY, 1483

Satellite formation stationkeeping represents a nontrivial application of novel dynamics and control. We explore the possibility of utilizing a flux-pinning connection to create a virtual structure that allows these maneuvers to become more feasible by augmenting the dynamics and passively stabilizing the relative position and orientation of the component satellites. We develop a mathematical framework for a generalized satellite formation along with expressions for the flux-pinning effect about established dynamic equilibria. This framework is then applied via simulation to a candidate ring-aperture telescope formation to examine the value of implementing a vehicle formation that is maintained through flux pinning.

I. Introduction

SATELLITE formations offer the promise of meeting requirements for space systems that must achieve large spatial extents, such as large-aperture telescopes. Physically separating components enables long-baseline observations and a large collecting aperture without the weight associated with interconnecting structure. Removing mechanical elements from among individual satellites also introduces opportunities for modularization^{1,2}. These advantages in turn likely reduce launch costs, extend system life, and simplify repair operations^{2,3}. However, by removing these mechanical connections entirely, one eliminates a simple and effective means of constraining the relative position among components, a disadvantage that the present study addresses.

Proposed means of overcoming this disadvantage focus mainly on active control, augmenting the dynamics of the system through additional physics, or a combination of the two. Through active control, a formation can maintain and modify relative positions and orientations of individual satellites, but typically at the expense of constant actuation, which may cost considerable fuel or power³⁻⁵. Berryman and Schaub describe a virtual Coulomb structure based on the attraction of charged particles⁶. Atchison and Peck propose specific types of formations by using the Lorentz force on a charged object in orbit around a planet with a magnetic field as an input⁷. Miller, Sedwick, and Kong suggest a solution based on electromagnetic attraction among actively controlled magnetic fields². The present study augments this list of possibilities by examining the feasibility of the flux-pinning effect between a magnetic field and a superconductor as a means of establishing action at a distance. The primary advantage of flux pinning over other approaches is that it creates a passively stable connection between two bodies. Any solution based on magnetic attraction alone—whether achieved by permanent magnets or electromagnets—cannot be described as passively stable. As a consequence of Earnshaw's Theorem, active control is generally necessary for a system of magnetically interacting components to maintain relative position or follow an arbitrary path⁸. Flux pinning sidesteps this issue by depending instead upon force generated on a magnet by a nearby superconductor that resists changes in the flux within its interior.

This resistance acts as a multiple degree-of-freedom spring and damper about some pinned position and orientation relative to the source of a magnetic field^{9,10}. In unactuated mechanical systems consisting of bodies interconnected by springs, masses, and dampers, we expect the total energy of the system never to increase, resulting in an asymptotically stable arrangement. By creating a similar arrangement in orbit, one can take advantage of this passively stable flux-pinning effect to establish a virtual structure that maintains relative position and orientation with reduced need for active control¹¹.

¹ Graduate Research Assistant, Sibley School of Mechanical and Aerospace Engineering, 127 Upson Hall, AIAA student member.

II. The Flux-Pinning Effect

Flux pinning refers to the interaction between a magnetic field and a high-temperature superconductor (HTSC). Motion of the magnetic field induces current vortices inside the HTSC, which then react to changes in the magnetic flux passing through the HTSC surface. The resistance within the HTSC is negligible under appropriate temperature conditions. So, these vortices persist for extended periods of time. This interaction establishes an equilibrium position and orientation of the magnetic field relative to the HTSC, in which perturbations are met with a restorative. This force is highly hysteretic: its instantaneous direction and magnitude depend upon the history of relative movement. For small motions, however, the flux-pinning reaction force resembles a linear, multiple degree-of-freedom spring-and-damper system. Perturbations from the initial state result in reaction forces and torques proportional to the relative displacement and velocity of the magnetic field and the HTSC.

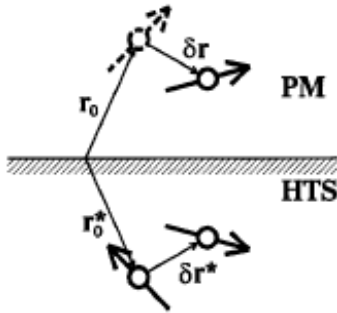


Figure 1. Illustration of the image model developed in Reference 15.

There are many approaches to finding force and torque expressions that have been presented in recent literature¹²⁻²¹. Approaching the force and torque interaction from an analytical point of view is often complicated by a lack of a convenient manner in which to express the currents and their derivatives induced in the HTSC surface. Nayau and Sanchez take this approach but require the magnet and superconductor to be cylindrical and to share an axis of symmetry^{16,17}. Others place similar constraints on the system described, resulting in an absence of general, analytical expressions for the force and torque interaction required for analysis and simulation.

Kordyuk addresses this issue by developing a model of a magnet and semi-infinite superconductor pair that approximates the interaction through the sum of two conceptual magnetic fields embedded in the HTSC. Figure 1 depicts the general concept of this model in the case of a permanent magnetic dipole. The permanent magnet is located by the vector r_0 . Cooling the HTSC past its critical temperature results in a conceptual image magnetic field fixed in the HTSC located by r_0^* formed by reflecting the initial magnetic moment over the HTSC plane and reversing its direction. Whereas the first image in the HTSC is fixed, the second image is mobile. Specifically, it is the reflection of the current magnetic moment, located by $r_0 + \delta r$, over the HTSC surface.

This image model conveniently predicts forces and torques associated with a magnetic dipole interacting with a semi-infinite plane HTSC suffering from no hysteresis or damping. As the magnetic field becomes more complex and the assumptions regarding the HTSC become less applicable, the model suffers. However, the model is appropriate for most configurations where the flux pinning effect represents a significant contribution to the total force and torque sum. Even so, the image model requires calculation of the interactions between at least three magnetic fields. Simplifying the model aids the tasks of designing and analyzing the dynamics of a flux-pinned connection. One possible model is that of a combined multiple degree of freedom spring, mass, and damper affecting translational and rotational motion. This particular simplified model is explored specifically by Shoer, Norman, and Peck⁹⁻¹¹.

Figure 2 shows a general layout of the vectors involved in expressions for this simplified model of the forces and torques. Coordinate frames are denoted by a script \mathcal{F} with an appropriate subscript and consist of a column matrix of three orthonormal basis vectors that comprise the frame. For example, the frame \mathcal{F}_a is defined as

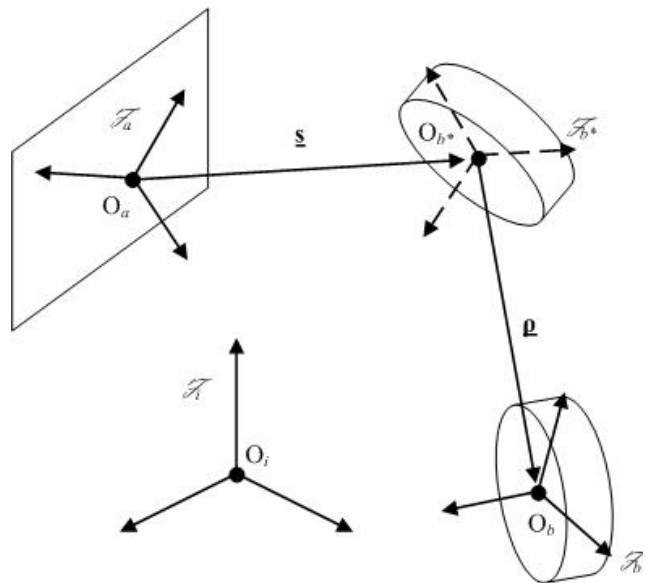


Figure 2. Flux-pinned connection between an HTSC and a magnetic dipole.

$$\mathcal{F}_a = [\mathbf{a}_1 \ \mathbf{a}_2 \ \mathbf{a}_3]^T \quad (1)$$

This notation offers a compact means of expressing vectors in terms of basis vectors of extracting the direction cosine matrix (DCM) between two frames²².

$$\mathbf{v} = \mathcal{F}_a \cdot \mathbf{y} \quad {}^a Q^b = \mathcal{F}_a \cdot \mathcal{F}_b^T \quad (2)$$

\mathcal{F}_i , shown in Fig. 2, establishes the inertial frame of reference. The point O_a locates the HTSC, and \mathcal{F}_a describes the associated fixed reference frame. Assuming a dipole representation for the magnetic field, the point O_b describes the position of the dipole. The frame \mathcal{F}_b is fixed to it with the third basis vector of \mathcal{F}_b parallel to the dipole axis. The flux pinning reaction depends upon the displacement and orientation of the magnetic field relative to an established equilibrium described by O_{b^*} and \mathcal{F}_{b^*} fixed with respect to the HTSC. These two quantities represent an “image” of the magnetic field where zero reaction force and torque occur due to flux pinning.

The translational restorative force applied to the magnetic field source is proportional to the relative position and velocity of the true location of O_b and its image, O_{b^*} . The inertial translational velocity of O_a , O_{b^*} , and O_b are \mathbf{v}_a , \mathbf{v}_{b^*} , and \mathbf{v}_b , and the angular velocity of the HTSC is $\underline{\omega}_a$. The vector from O_a to O_{b^*} is the vector $\underline{\mathbf{s}}$ fixed in \mathcal{F}_a , and the vector $\underline{\mathbf{p}}$ points from O_{b^*} to O_b . The linearized stiffness and damping are given by the dyadics $\underline{\mathbf{K}}$ and $\underline{\mathbf{C}}$. The restorative force is then

$$\begin{aligned} \underline{\mathbf{f}}_{ab} &= -\underline{\mathbf{K}} \cdot \underline{\mathbf{p}} - \underline{\mathbf{C}} \cdot (\mathbf{v}_b - \mathbf{v}_{b^*}) \\ &= -\underline{\mathbf{K}} \cdot \underline{\mathbf{p}} - \underline{\mathbf{C}} \cdot [\mathbf{v}_b - (\mathbf{v}_a + \underline{\omega}_a \times \underline{\mathbf{s}})] \end{aligned} \quad (3)$$

Describing the reaction torque involves examining the relative orientation of the magnetic field and its image fixed with respect to the HTSC. Again utilizing the dipole assumption, rotations about the dipole axis result in no change in the flux distribution in the HTSC, implying no stiffness and damping about this rotational axis. This property of rotationally symmetric magnetic fields has been observed in experimentation⁹. The restorative torque can then be expressed as proportional to the cross product between the dipole axis of the image magnet $\underline{\mathbf{b}}_3^*$ and the real magnet $\underline{\mathbf{b}}_3$ and to the difference of the angular velocity projected onto a plane normal to the $\underline{\mathbf{b}}_3$ axis. This relation leads to the following expression for the torque applied to the magnet by the HTSC via flux pinning, $\underline{\mathbf{g}}_{ab}$:

$$\underline{\mathbf{g}}_{ab} = -D \underline{\mathbf{b}}_3 \times \underline{\mathbf{b}}_3 - B (\underline{\mathbf{b}}_1 \underline{\mathbf{b}}_1 + \underline{\mathbf{b}}_2 \underline{\mathbf{b}}_2) \cdot (\underline{\omega}_b - \underline{\omega}_a) \quad (4)$$

The stiffness and damping coefficients $\underline{\mathbf{K}}$, D , $\underline{\mathbf{C}}$, and B are functions of the pinned location and orientation of O_{b^*} and \mathcal{F}_{b^*} relative to O_a and \mathcal{F}_a . So, they are functions of $\underline{\mathbf{s}}$ and ${}^a Q^{b^*}$. The stiffness afforded by flux pinning drops exponentially with increasing separation of the magnetic field and the HTSC, limiting the effective range of the connection to distances on the order of tens of cm for modest superconductor and magnet masses. References 9 and 10 provide further insight into experimentally derived values of these coefficients for specific configurations, along with curve fits used to predict their values at other points.

III. Mathematical Construction

Having introduced the concept of flux pinning and the mathematical model used to describe its effects, we apply it to a model of a multi-body structure in orbit representing a generalized satellite formation. This process involves developing the equations of motion. We consider N rigid bodies connected via arbitrary force and torque relations. Let the vector $\underline{\mathbf{r}}$, originating from a reference point O , represent an arbitrary position vector. Time derivatives in the inertial frame are denoted by an over-dot. A reference point on each rigid body is located by vector $\underline{\mathbf{b}}_n$ extending from O to a point O_n in body R_n and its associated reference frame \mathcal{F}_n . From these starting points we can define a vector $\underline{\mathbf{r}}_n$, which is fixed in \mathcal{F}_n :

$$\underline{\mathbf{r}} = \underline{\mathbf{r}}_n + \underline{\mathbf{b}}_n \quad (5)$$

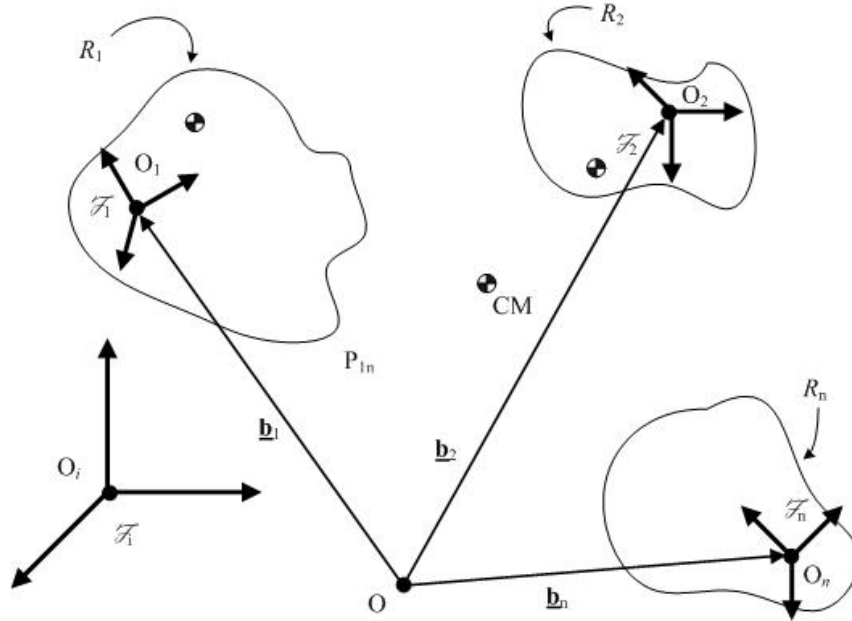


Figure 3. N-body satellite formation

The momentum of R_n is determined by the angular velocity vector $\underline{\omega}_n$ and the inertial velocity vector \underline{v}_n . The velocity of an arbitrary point in the inertial frame is then given via the transport theorem:

$$\underline{v}(\underline{r}) = \underline{v}_n + \underline{\omega}_n \times \underline{r}_n \quad (6)$$

The mass center of the nth body is

$$\underline{c}_n = \int_{R_n} \underline{r}_n dm \quad (7)$$

and its inertia dyadic is

$$\underline{\underline{J}}_n = \int_{R_n} (\underline{r}_n \cdot \underline{r}_n \underline{\underline{1}} - \underline{r}_n \underline{r}_n) dm \quad (8)$$

These definitions appear in the equations of motion, derived from Newton's second law: the time derivative of the momentum vectors of each body equal the external forces and moments applied. The momentum of the nth body, in terms of its angular velocity, translational velocity, mass, and first moment of inertia, is

$$\underline{p}_n = \int_{R_n} \underline{v} dm = \int_{R_n} (\underline{v}_n + \underline{\omega}_n \times \underline{r}_n) dm = m_n \underline{v}_n + \underline{\omega}_n \times \underline{c}_n \quad (9)$$

Similarly, the angular momentum of R_n in terms of its first and second moments of inertia, velocity of the point O_n , and the angular velocity of R_n , is

$$\begin{aligned} \underline{h}_n &= \int_{R_n} \underline{r}_n \times \underline{v} dm = \int_{R_n} \underline{r}_n \times (\underline{v}_n + \underline{\omega}_n \times \underline{r}_n) dm = \int_{R_n} \underline{r}_n \times \underline{v}_n dm + \int_{R_n} \underline{r}_n \times \underline{\omega}_n \times \underline{r}_n dm \\ &= \underline{c}_n \times \underline{v}_n + \underline{\underline{J}}_n \cdot \underline{\omega}_n \end{aligned} \quad (10)$$

The inertial time derivative of the momentum is

$$\dot{\underline{\mathbf{p}}}_n = \underline{\mathbf{F}}_n = \underline{\mathbf{f}}_n - \sum_{j=1}^{n-1} \underline{\mathbf{f}}_{jn} + \sum_{j=n+1}^N \underline{\mathbf{f}}_{nj} \quad (11)$$

The inertial time derivative of the angular momentum leads to

$$\begin{aligned} \dot{\underline{\mathbf{h}}}_n + \underline{\mathbf{v}}_n \times \underline{\mathbf{p}}_n &= \underline{\mathbf{G}}_n \\ \dot{\underline{\mathbf{h}}}_n + \underline{\mathbf{v}}_n \times (m_n \underline{\mathbf{v}}_n + \underline{\omega}_n \times \underline{\mathbf{c}}_n) &= \underline{\mathbf{g}}_n - \sum_{j=1}^{n-1} \underline{\mathbf{g}}_{jn} + \sum_{j=n+1}^N \underline{\mathbf{g}}_{nj} - \sum_{j=1}^{n-1} \underline{\mathbf{d}}_{nj} \times \underline{\mathbf{f}}_{jn} + \sum_{j=n+1}^N \underline{\mathbf{d}}_{nj} \times \underline{\mathbf{f}}_{nj} \\ \dot{\underline{\mathbf{h}}}_n &= \underline{\mathbf{g}}_n - \sum_{j=1}^{n-1} (\underline{\mathbf{g}}_{jn} + \underline{\mathbf{d}}_{nj} \times \underline{\mathbf{f}}_{jn}) + \sum_{j=n+1}^N (\underline{\mathbf{g}}_{nj} + \underline{\mathbf{d}}_{nj} \times \underline{\mathbf{f}}_{nj}) \\ &\quad - (\underline{\mathbf{v}}_n \cdot \underline{\mathbf{c}}_n \underline{\mathbf{1}} - \underline{\mathbf{c}}_n \underline{\mathbf{v}}_n) \cdot \underline{\omega}_n \end{aligned} \quad (12)$$

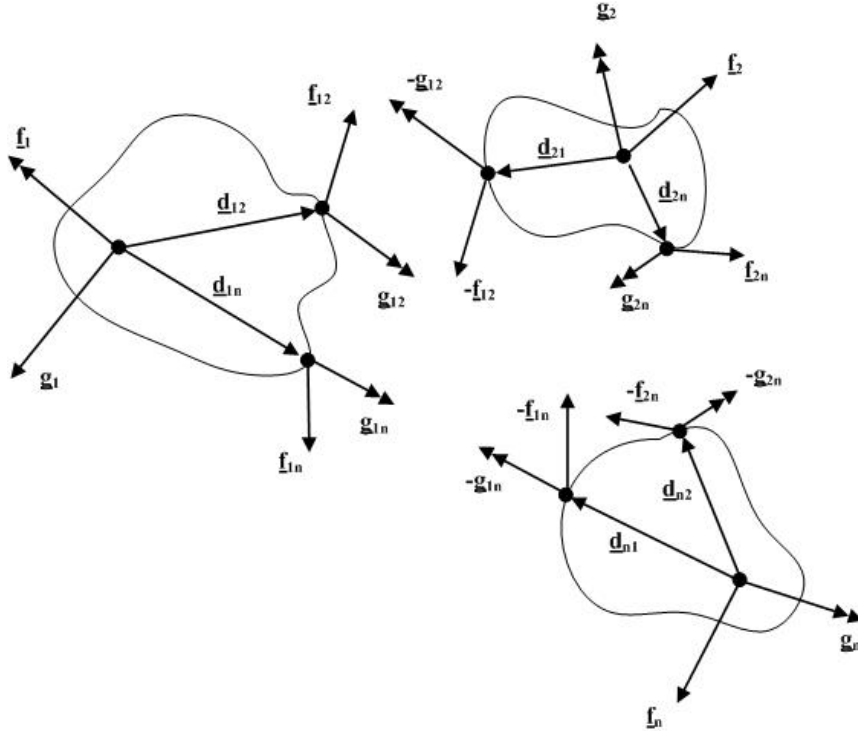


Figure 4. Free-body diagram of an N-body satellite formation.

The forces and torques applied to body R_1 by the other bodies in the system by the convention adopted here are defined as positive. The forces and torques applied to next body, R_2 , include the opposite of the previously described $\underline{\mathbf{f}}_{12}$ and $\underline{\mathbf{g}}_{12}$ along with the new force and torque relations to each other body in the system. This convention continues until the last body, R_N , where all forces and torques are as previously defined. In terms of the \mathcal{F}_n vectrix,

$$\begin{aligned} & \left[\underline{\mathbf{v}}_n \ \underline{\omega}_n \ \underline{\mathbf{c}}_n \ \underline{\mathbf{p}}_n \ \underline{\mathbf{h}}_n \ \underline{\mathbf{f}}_n \ \underline{\mathbf{f}}_{n+1} \ \cdots \ \underline{\mathbf{f}}_{nN} \ \underline{\mathbf{g}}_n \ \underline{\mathbf{g}}_{n+1} \ \cdots \ \underline{\mathbf{g}}_{nN} \right] \\ &= \mathcal{F}_n \cdot \left[\underline{\mathbf{v}}_n \ \underline{\omega}_n \ \underline{\mathbf{c}}_n \ \underline{\mathbf{p}}_n \ \underline{\mathbf{h}}_n \ \underline{\mathbf{f}}_n \ \underline{\mathbf{f}}_{n+1} \ \cdots \ \underline{\mathbf{f}}_{nN} \ \underline{\mathbf{g}}_n \ \underline{\mathbf{g}}_{n+1} \ \cdots \ \underline{\mathbf{g}}_{nN} \right] \end{aligned} \quad (13)$$

$$\underline{\mathbf{J}}_n = \mathcal{F}_n \cdot \underline{\mathbf{J}}_n \cdot \mathcal{F}_n^T \quad (14)$$

\mathbf{J}_n is constant in the F_N axes. The expression for momentum of R_n becomes

$$\begin{aligned}\mathbf{p}_n &= \mathcal{F}_n \cdot \underline{\mathbf{p}}_n = \mathcal{F}_n \cdot (m_n \underline{\mathbf{v}}_n + \underline{\boldsymbol{\omega}}_n \times \underline{\mathbf{c}}_n) \\ &= m_n \underline{\mathbf{v}}_n - \underline{\mathbf{c}}_n \times \underline{\boldsymbol{\omega}}_n\end{aligned}\quad (15)$$

The inertial time derivative of this momentum can also be expressed in the \mathcal{F}_n frame

$$\begin{aligned}\dot{\mathbf{p}}_n &= \mathcal{F}_n \cdot \dot{\underline{\mathbf{p}}}_n = \mathcal{F}_n \cdot \left(\underline{\mathbf{f}}_n - \sum_{j=1}^{n-1} \underline{\mathbf{f}}_{jn} + \sum_{j=n+1}^N \underline{\mathbf{f}}_{nj} \right) \\ &= \underline{\mathbf{f}}_n - \sum_{j=1}^{n-1} \mathcal{F}_n \cdot \mathcal{F}_j^T \underline{\mathbf{f}}_{jn} + \sum_{j=n+1}^N \underline{\mathbf{f}}_{nj} \\ &= \underline{\mathbf{f}}_n - \sum_{j=1}^{n-1} {}^n Q^j \underline{\mathbf{f}}_{jn} + \sum_{j=n+1}^N \underline{\mathbf{f}}_{nj}\end{aligned}\quad (16)$$

where ${}^n Q^j$ represents the direction cosine matrix from \mathcal{F}_j to \mathcal{F}_n . Similarly, the expression for the angular momentum of the n th body becomes

$$\mathbf{h}_n = \mathcal{F}_n \cdot \underline{\mathbf{h}}_n = \mathcal{F}_n \cdot (\underline{\mathbf{c}}_n \times \underline{\mathbf{v}}_n + \underline{\mathbf{J}}_n \cdot \underline{\boldsymbol{\omega}}_n) = \underline{\mathbf{c}}_n \times \underline{\mathbf{v}}_n + \underline{\mathbf{J}}_n \underline{\boldsymbol{\omega}}_n \quad (17)$$

and its inertial time derivative is

$$\begin{aligned}\dot{\mathbf{h}}_n &= \mathcal{F}_n \cdot \dot{\underline{\mathbf{h}}}_n \\ &= \mathcal{F}_n \cdot \left[\underline{\mathbf{g}}_n - \sum_{j=1}^{n-1} (\underline{\mathbf{g}}_{jn} + \underline{\mathbf{d}}_{nj} \times \underline{\mathbf{f}}_{jn}) + \sum_{j=n+1}^N (\underline{\mathbf{g}}_{nj} + \underline{\mathbf{d}}_{nj} \times \underline{\mathbf{f}}_{nj}) - (\underline{\mathbf{v}}_n \cdot \underline{\mathbf{c}}_n \underline{\mathbf{1}} - \underline{\mathbf{c}}_n \underline{\mathbf{v}}_n) \cdot \underline{\boldsymbol{\omega}}_n \right] \\ &= \underline{\mathbf{g}}_n - \sum_{j=1}^{n-1} [\mathcal{F}_n \cdot \mathcal{F}_j^T \underline{\mathbf{g}}_{jn} + \mathcal{F}_n \cdot \mathcal{F}_j^T \underline{\mathbf{d}}_{nj} \times (\mathcal{F}_n \cdot \mathcal{F}_j^T \underline{\mathbf{f}}_{jn})] + \sum_{j=n+1}^N (\underline{\mathbf{g}}_{nj} + \underline{\mathbf{d}}_{nj} \times \underline{\mathbf{f}}_{nj}) \\ &\quad - (\underline{\mathbf{v}}_n^T \underline{\mathbf{c}}_n \underline{\mathbf{1}} - \underline{\mathbf{c}}_n \underline{\mathbf{v}}_n^T)^T \underline{\boldsymbol{\omega}}_n \\ &= \underline{\mathbf{g}}_n - \sum_{j=1}^{n-1} [{}^n Q^j \underline{\mathbf{g}}_{jn} + \underline{\mathbf{d}}_{nj} \times {}^n Q^j \underline{\mathbf{f}}_{jn}] + \sum_{j=n+1}^N (\underline{\mathbf{g}}_{nj} + \underline{\mathbf{d}}_{nj} \times \underline{\mathbf{f}}_{nj}) - \underline{\mathbf{v}}_n \times \underline{\boldsymbol{\omega}}_n \times \underline{\mathbf{c}}_n\end{aligned}\quad (18)$$

$\underline{\mathbf{F}}_n$ and $\underline{\mathbf{G}}_n$ describe the forces and torques, respectively, applied to each body

$$\underline{\mathbf{F}}_n = \underline{\mathbf{f}}_n - \sum_{j=1}^{n-1} {}^n Q^j \underline{\mathbf{f}}_{jn} + \sum_{j=n+1}^N \underline{\mathbf{f}}_{nj} \quad (19)$$

$$\underline{\mathbf{G}}_n = \underline{\mathbf{g}}_n - \sum_{j=1}^{n-1} [{}^n Q^j \underline{\mathbf{g}}_{jn} + \underline{\mathbf{d}}_{nj} \times {}^n Q^j \underline{\mathbf{f}}_{jn}] + \sum_{j=n+1}^N (\underline{\mathbf{g}}_{nj} + \underline{\mathbf{d}}_{nj} \times \underline{\mathbf{f}}_{nj}) \quad (20)$$

The dynamics are then parameterized by

$$\mathcal{A} = [\mathbf{p}_1^T \cdots \mathbf{p}_N^T \mathbf{h}_1^T \cdots \mathbf{h}_N^T]^T \quad (21)$$

$$\mathcal{A} = [\mathbf{v}_1^T \cdots \mathbf{v}_N^T \ \omega_1^T \cdots \omega_N^T]^T \quad (22)$$

$$\mathcal{A} = [\mathbf{F}_1^T \cdots \mathbf{F}_N^T \ \mathbf{G}_1^T \cdots \mathbf{G}_N^T]^T \quad (23)$$

$$\mathcal{A}_p = [0 \cdots 0 (\mathbf{v}_1^\times \omega_1^\times \mathbf{c}_1)^T \cdots (\mathbf{v}_N^\times \omega_N^\times \mathbf{c}_N)^T]^T \quad (24)$$

$$\mathcal{M} = \begin{bmatrix} m_1 \mathbf{1} \cdots \mathbf{0} & -\mathbf{c}_1^\times \cdots \mathbf{0} \\ \vdots & \vdots \\ \mathbf{0} \cdots m_N \mathbf{1} & \mathbf{0} \cdots -\mathbf{c}_N^\times \\ \mathbf{c}_1^\times \cdots \mathbf{0} & \mathbf{J}_1 \cdots \mathbf{0} \\ \vdots & \vdots \\ \mathbf{0} \cdots \mathbf{c}_N^\times & \mathbf{0} \cdots \mathbf{J}_N \end{bmatrix} \quad (25)$$

The equation of motion is then

$$\dot{\mathcal{h}} = \mathcal{A} + \mathcal{A}_p \quad (26)$$

\mathcal{M} is the transformation from the dynamic variables \mathcal{A} to the kinematic variables \mathcal{A}

$$\mathcal{h} = \mathcal{M}\mathcal{A} \quad (27)$$

If O_n is made to be coincident with the center of mass of R_n , the \mathbf{c}_n terms reduce to zero, simplifying Eq. (26) by reducing the complexity of the \mathcal{A}_p and \mathcal{M} matrices.

In addition to the flux-pinning forces, electromagnetic interaction between the magnetic dipoles representing half of the flux-pinning hardware may impart forces and torques. Landecker, Villani, and Yung offer an approximation of these reactions in terms of the magnetic moments and their relative position²³.

$$\mathbf{f}_{nj} = \frac{3\mu_0}{4\pi(\mathbf{r} \cdot \mathbf{r})^2} \left\{ (\hat{\mathbf{r}} \times \mathbf{m}_n) \times \mathbf{m}_j + (\hat{\mathbf{r}} \times \mathbf{m}_j) \times \mathbf{m}_n + \hat{\mathbf{r}} [5(\hat{\mathbf{r}} \times \mathbf{m}_n) \cdot (\hat{\mathbf{r}} \times \mathbf{m}_j) - 2\mathbf{m}_n \cdot \mathbf{m}_j] \right\} \quad (28)$$

$$\mathbf{g}_{nj} = \frac{\mu_0 \sqrt{(\mathbf{m}_n \cdot \mathbf{m}_n)(\mathbf{m}_j \cdot \mathbf{m}_j)}}{4\pi \sqrt{(\mathbf{r} \cdot \mathbf{r})^3}} \left[3(\hat{\mathbf{m}}_n \cdot \hat{\mathbf{r}})(\hat{\mathbf{m}}_j \times \hat{\mathbf{r}}) + \hat{\mathbf{m}}_n \times \hat{\mathbf{m}}_j \right] \quad (29)$$

where \mathbf{m}_n represents the magnetic moment of the dipole at P_{nj} , \mathbf{r} represents the vector from P_{nj} to P_{jn} , and the circumflex indicates a unit vector. In some configurations, the electromagnetic attraction between the dipoles may be negligible compared to the flux-pinning effect, but if the formation requires these points to be in close proximity, these forces may be relevant.

The model also needs an expression for the external forces and torques applied to R_n at O_n , \mathbf{f}_n and \mathbf{g}_n , respectively. These forces represent a sum of gravitational effects and control inputs. The force and torque due to gravity on R_n applied at the body's center of mass are:

$$\mathbf{f}_n = -\mu \int_{R_n} \frac{\mathbf{R} dm}{\sqrt{\mathbf{R} \cdot \mathbf{R}}^3} \quad (30)$$

$$\mathbf{g}_n = -\mu \int_{R_n} \frac{\mathbf{r} \times \mathbf{R} dm}{\sqrt{\mathbf{R} \cdot \mathbf{R}}^3} \quad (31)$$

where \mathbf{R} points from the gravitational primary to a point inside R_n and \mathbf{r} points from the center of mass of R_n to the same point. If O_n is not the center of mass of R_n , then the torque applied at the center of mass must be referenced to the appropriate point. The control inputs of the formation are left unspecified, as they depend on the particular formation being described. The forces and torques applied to the body through \mathcal{J} depend upon the relative orientations of the bodies and their particular components. The relative attitudes of the bodies orient the vectors described above, allowing computation of the flux-pinning effect.

IV. Example Formation

Here, this mathematical model is used in a specific example in order to demonstrate the concept's promise for passive stationkeeping. The example is that of a sparse-aperture space telescopes. The concept of utilizing formation flight for enhanced telescope imaging capabilities is a topic of current interest²⁴⁻²⁶. By separating portions of the telescope spatially, we effectively increase the aperture of the telescope without reducing its light-gathering capability. The specific layout of the individual satellites depends on the science objectives of the telescope, along with the wavelength of light of interest; in this case, the architecture is that of the ring formation conceived for in Ref. 25. Its mission is to observe in x-ray wavelengths. We consider an optical analogue of this mission.

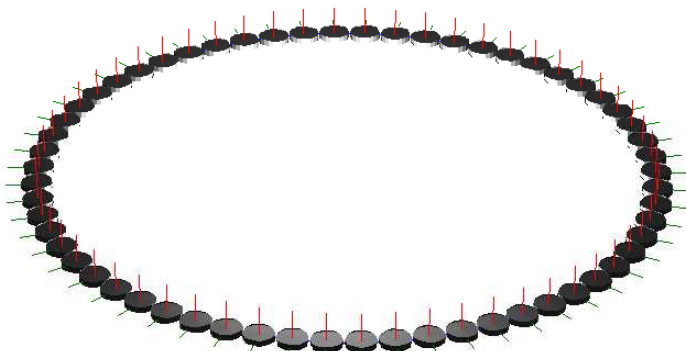


Figure 5. Example sparse ring aperture formation.

A particular form of sparse aperture telescope is that of a ring aperture, where mirror segments, or individual telescopes, are placed on a circle about a central detector in a plane perpendicular to the target imaging direction. A ring aperture telescope has a few key advantages: redundant UV-plane coverage and identical design of mirror modules. Here, each mirror module is also a vehicle. The first advantage addresses the concern of assembling an image from a sparse-aperture telescope. While other designs maximize UV-plane coverage in order to avoid loss of information at different spatial frequencies with a minimum number of vehicles, a ring aperture has redundancies in the UV-plane coverage, resulting in a simplified diffraction image²⁶. As all of the ring vehicles are at the same distance and in the same normal plane relative to the central detector, each vehicle can be identical to each other. This is conceptually different from other arrangements in which the mirror segment on each module corresponds in a gross manner to a particular location due to the varying reflection properties. As an ideal ring aperture is rotationally symmetric, we avoid this problem.

The ring's vehicles consist of a spacecraft bus attached to a mirror actuation and control module, identical flux-pinning connections consisting of an arrangement of permanent magnets, electromagnets, superconductors, and a cooling system, and an appropriate configuration of relative actuators to control the

spatial frequencies with a minimum number of vehicles, a ring aperture has redundancies in the UV-plane coverage, resulting in a simplified diffraction image²⁶. As all of the ring vehicles are at the same distance and in the same normal plane relative to the central detector, each vehicle can be identical to each other. This is conceptually different from other arrangements in which the mirror segment on each module corresponds in a gross manner to a particular location due to the varying reflection properties. As an ideal ring aperture is rotationally symmetric, we avoid this problem.

Table 1. Example Formation Parameters

Ring Vehicle Parameters

| | | | |
|------------------------------------|-----------------|--------|---------|
| Total Mass (kg) | 100 | | |
| Bounding Box Dimensions (m) | 1.0 x 1.0 x 0.2 | | |
| Inertia Matrix (kgm ²) | 6.5833 | 0 | 0 |
| | 0 | 6.5833 | 0 |
| | 0 | 0 | 12.5000 |

Table 2. Assumed flux pinning parameters

Assumed stiffness at 4.8cm separation

| | |
|---|----------|
| Vertical translational stiffness (relative to HTSC surface) | 10 N/m |
| Lateral translational stiffness (relative to HTSC surface) | 5 N/m |
| Rotational stiffness (relative to pinned orientation) | 4 Nm/rad |

Assumed damping at 4.8cm separation

| | |
|---|------------|
| Vertical translational damping (relative to HTSC surface) | 1 Ns/m |
| Lateral translational damping (relative to HTSC surface) | 0.5 Ns/m |
| Rotational damping (relative to pinned orientation) | 0.4 Nm/rad |

separation from the center vehicle. The flux-pinning interface joins the individual modules together to form the virtual ring structure in a non-contacting manner. On top of these coupled vehicle dynamics, each mirror vehicle is individually controlled in order to regulate radial position relative to the center module in the presence of disturbances and reconfiguration commands. The inputs to these ring modules are in the form of relative action at a distance, such as the electromagnetic formation flight (EMFF) concept of Miller² or Schaub's Coulomb virtual structure⁶. A central detector vehicle not depicted in Fig. 5 collects the reflections from the individual mirror vehicles. The presence of such a vehicle aids the relative navigation and control scheme by providing a reference relative to which the ring vehicles can detect their distance and orientation, allowing for a control scheme to be developed.

Our simulation focuses on this concept of a ring aperture telescope application with a nominal ring radius of 20-m and 60 vehicles, which in combination with the ring vehicle parameters listed in Table 1 implies an approximate separation distance of 4.8 cm between the flux pinning components of neighboring vehicles. Reasonable stiffness and damping values can be obtained at this distance^{9,10}. The simulation implements a stiffness and damping model to determine the relative forces between the spacecraft.

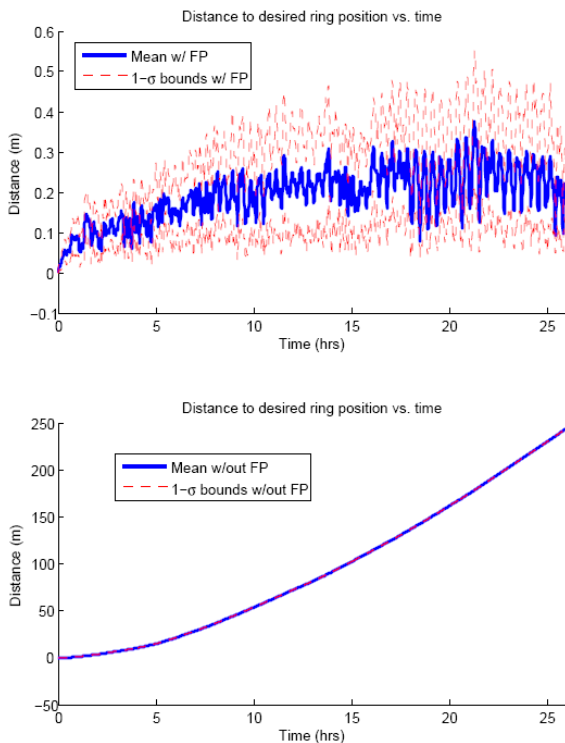


Figure 7. Plots demonstrating statistical vehicle position error of the flux-pinned and unlinked formations as a result of force and torque input disturbances.

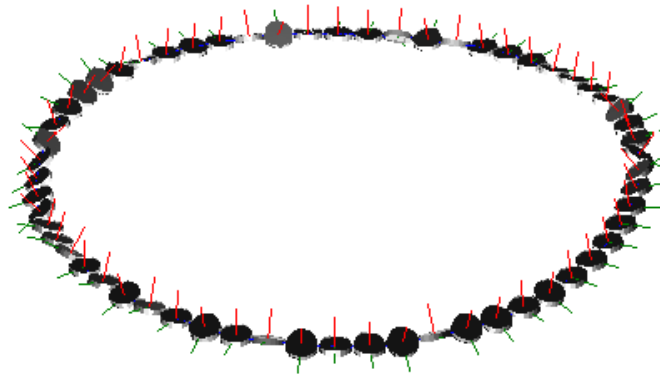


Figure 6. Simulated vehicle positions at t=29 hours with flux pinning dynamically linking neighboring vehicles

The values of these parameters are listed in Table 2. The simulation neglects gravitational effects, making it appropriate for spacecraft far from any significant gravitational field.

A. Simulation Results

The objective of the simulation presented in this paper is to demonstrate the value of a flux-pinned formation to space-based applications. The first simulation focuses on examining the candidate ring formation in the presence of input force and torque disturbances with no forces among the satellites. The second introduces a flux-pinned connection between neighboring vehicles. The input disturbance in both cases is modeled with a zero mean Gaussian distribution with a standard deviation of $1 \mu\text{N}$ or $\mu\text{N}\cdot\text{m}$. As expected, the input disturbances applied to the unconnected formation result in each vehicle proceeding in a random walk from its initial position and orientation, ultimately leading to an unorganized collection of bodies. By comparison, the flux-pinned formation maintained a relatively collected arrangement, as shown in Fig. 6. Figure 7 plots statistics relevant to the simulation performances, namely the mean and $1\text{-}\sigma$ bounds of the translational distance of the vehicles to a ring centered on the formation center of mass and perpendicular to the major axis of inertia of the collection of vehicles as a whole. This plot demonstrates that the addition of flux

pinning greatly aided in keeping the vehicles closer to their intended location when compared to the dynamically unlinked case.

Reference 11 suggests that given that the ring vehicles are close enough to effectively sustain a flux pinning interface, they should stay in relative proximity throughout an orbital period. While staying in proximity is an important function of a space structure, a space-telescope application requires precise control of individual vehicle positions relative to the detector. In the absence of control inputs, a flux-pinned connection would shift equilibrium positions in the presence of disturbances or time-varying external forces without some form of feedback control.

B. Control Implementation

Spacecraft formation control represents a large and active area of research²⁷⁻³⁸ generally beyond the scope of this paper. One attractive option is Model Predictive Control (MPC). MPC represents a finite-horizon discrete time optimal control algorithm, and has been the subject of much research as applied to nonlinear systems over the past decade²⁹⁻³⁸. References 32-38 deal with the particular problem of applying MPC to spacecraft attitude and formation control. The value of MPC lies in the easy extensions to incorporating discrete time extended Kalman filters, hard control and dynamics constraints, incorporation of nonlinear dynamics, and performance-driven input optimization. Historically, MPC has found most of its applications in control of slowly-changing industrial and chemical processes, as predicting the dynamics significantly forward in time can result in substantial computational overhead. The increased available computation power in smaller systems has recently made MPC a viable option for performance-driven control in robotics and spacecraft applications.

An MPC control scheme would be particularly well-suited to the stationkeeping and reconfiguration of a ring-aperture flux-pinned telescope, as the control input optimization scheme for the servo problem can be posed in terms of tracking performance metrics as opposed to state trajectories. Three important performances of the proposed formation would be the radial distance of a vehicle from the central detector, its velocity in the same radial direction, and its distance from the imaging plane. As these metrics do not describe any motion perpendicular to the radial direction and the normal of the imaging plane, the vehicle is free to move in a specified diameter ring existing in the imaging plane. Figure 10 describes the associated performance time histories of a single 100kg vehicle utilizing an MPC control scheme with those three performances to match a 10-m radius ring about a central body. Incorporating this control scheme into a multi-body flux-pinned simulation represents the subject of future work.

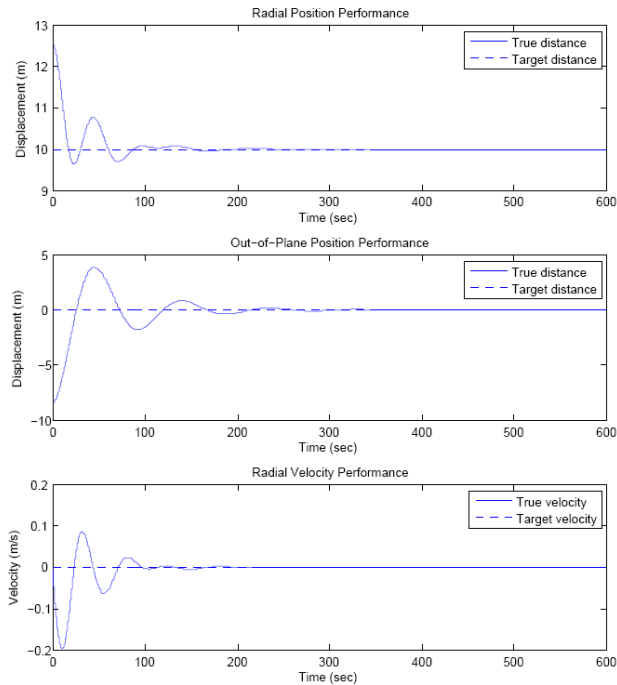


Figure 8. MPC Simulation performances for a single 100kg body to move to a specified 10-m ring from an arbitrary initial state.

V. Conclusion

By establishing a passively stable connection between individual spacecraft in a formation, flux pinning creates a virtual structure upon which one can implement standard control laws to accomplish the typical tasks of station keeping and reconfiguration. The passive stability of the formation without active control provides a safety net, guaranteeing that in the absence of control inputs the formation remains intact despite different orbital parameters for individual spacecraft. This useful quality has potential to simplify the mechanical design of future satellite formations^{11,24,39}.

In the proposed conceptual framework, the reconfiguration task displaces the spacecraft from their flux-pinned equilibrium states, resulting in a restorative force attempting to return them to the original formation. This effect typically requires feedback control in order to maintain the new formation at a level of precision appropriate for an optical system. The design can take advantage of the temperature-dependent properties of flux pinning to reset the

connections and define new equilibrium states corresponding to the newly reconfigured formation. Once the reconfigured state is reached, the spacecraft can temporarily raise the temperature of the superconductors past their critical temperature, effectively clearing the flux-pinning connection. Subsequently re-freezing the superconductors “resets” the pinned equilibrium positions of the nearby magnetic fields to their current configuration in the reconfigured system.

This simulation does not model the hysteretic effects associated with flux pinning. However, hysteresis can be exploited to allow the pinned equilibrium point to be shifted without thawing and refreezing, changing the equilibrium configuration along with the linearized stiffness and damping coefficients. A mathematical model of these changes can allow the spacecraft’s operations concept to incorporate them into the reconfiguration process. The type of HTSC material on which the connection is based also modifies the magnitude of the hysteretic effect. Additionally, the effect of actively controlling the magnetic fields involved in flux pinning may result in similar modification of the properties of the equilibrium state in a flux-pinned connection. Future work would include examining these potential interactions, along with designing control strategies which would take advantage of the additional relative dynamics introduced by flux pinning between bodies in the formation. These directions for future work hold promise for the use of this technology in reconfiguration of modular spacecraft.

References

- ¹DARPA BAA 07-31, System F6, Jul. 16, 2007.
- ²Miller, D.W., R. J. Sedwick, and E. M. C. Kong, “Electromagnetic formation flight for sparse aperture telescopes,” *IEEE Aerospace Conference Proceedings*, IEEE, Piscataway, New Jersey, Vol. 2, 2002 pp. 2-729- 2-741.
- ³Inalhan, G., M. Tillerson, and J. P. How, “Relative dynamics and control of spacecraft Formations in eccentric orbits”, *Journal of Guidance, Control, and Dynamics*, Vol. 25, No. 1, Jan-Feb 2002 pp. 48-59.
- ⁴Hamel, J. F., and J. de Lafontaine, “Neighboring optimum feedback control law for Earth-orbiting formation flying,” *AAS/AIAA Astrodynamics Specialist Conference*, AAS/AIAA, Mackinac Island, MI, 19-23 Aug. 2007.
- ⁵Ulybyshev, Y., “Long-term formation keeping of satellite constellation using linear-quadratic controller,” *Journal of Guidance, Control, and Dynamics*, Vol. 21, No. 1, Jan-Feb 1998 pp. 109-115.
- ⁶Berryman, J. and H. Schaub, “Analytical charge analysis for two- and three-craft coulomb formations,” *Journal of Guidance, Control, and Dynamics*, Vol. 30, No. 6, Nov.-Dec. 2007.
- ⁷Atchison, J., and M. Peck, “A millimeter-scale Lorentz-propelled spacecraft,” *AIAA Guidance, Navigation and Control Conference*, AIAA, Hilton Head, SC, 20-23 Aug. 2007.
- ⁸Earnshaw, S., “On the nature of the molecular forces which regulate the constitution of the luminiferous ether,” *Transactions of the Cambridge Philosophical Society*, Vol. 7, Part I, 1842, pp. 97-112.
- ⁹Shoer, J. and M. Peck, “A flux-pinned magnet-superconductor pair for close-proximity station keeping and self-assembly of spacecraft,” *AIAA Guidance, Navigation, and Control Conference*, AIAA, Hilton Head, SC, 19-20 Aug. 2007.
- ¹⁰Shoer, J. and M. Peck, “Flux-pinned interfaces for the assembly, manipulation, and reconfiguration of modular space systems,” *AIAA Guidance, Navigation, and Control Conference*, AIAA, Honolulu, HI, 18-21 Aug. 2008.
- ¹¹Norman, M., and M. A. Peck, “Modeling and properties of a flux-pinned network of satellites,” *AAS/AIAA Astrodynamics Specialist Conference*, AAS, Mackinac Island, MI, 19-23 Aug. 2007.
- ¹²Chang, P.Z., F.C. Moon, J. R. Hull, and T. M. Mulcahy, “Levitation force and magnetic stiffness in bulk high-temperature superconductors,” *Journal of Applied Physics*, Vol. 67, No. 9, 1990, pp. 4358-4360.
- ¹³Hull, J. R. and A. Cansiz, “Vertical and lateral forces between a permanent magnet and a high-temperature superconductor”, *Journal of Applied Physics*, Vol. 86, No. 11, 1999, pp. 6396-6404.
- ¹⁴Johansen, T. H., H. Mestl, and H. Bratsberg, “Investigation of the lateral magnetic force and stiffness between a high- T_c superconductor and magnet of rectangular shapes”, *Journal of Applied Physics*, Vol. 75, No. 3, 1994, pp. 1667-1670.
- ¹⁵Kordyuk, A. A., “Magnetic levitation for hard superconductors”, *Journal of Applied Physics*, Vol. 83, No. 1, 1998, pp. 610-613.
- ¹⁶Navau, C., and A. Sanchez, “Magnetic properties of finite superconducting cylinders. I. Uniform applied field”, *Phys. Rev. B*, Vol. 64, No. 21, 2001, pp. 214506.
- ¹⁷Sanchez, A., and C. Navau, “Magnetic properties of finite superconducting cylinders. II. Nonuniform applied field and levitation force”, *Phys. Rev. B*, Vol. 64, No. 21, 2001, pp. 214507.
- ¹⁸Tsuchimoto, M, T. Kojima, H. Takeuchi, and T. Honma, “Numerical analyses of levitation force and flux creep on high T_c superconductor”, *IEEE Transactions on Magnetism*, Vol. 29, No. 6, 1993, pp. 3577-3579.
- ¹⁹Weeks, D. E. “Levitation properties of the $YBa_2Cu_3O_x$ and $Tl-Ba-Ca-Cu-O$ superconduction systems”, *Applied Physics Letters*, Vol. 55, No. 26, 1989, pp. 2784-2786.
- ²⁰Yamachi, N., T. Nishikawa, N. Sakai, K. Sawa, and M. Murakami, “Levitation forces of bulk superconductors in varying fields”, *Physica C*, 2003, pp. 579-584.
- ²¹Yang, Z. J., and J. R. Hull, “Effect of size on levitation force in a magnet/superconductor system”, *Journal of Applied Physics*, Vol. 79, No. 6, 1996, pp. 3318-3321.
- ²²Hughes, P. C., *Spacecraft Attitude Dynamics*, Dover Publications, Inc., Mineola, New York, 2004, pp. 522-534.

- ²³Landecker, P. B, Villani, D. D., and K. W. Yung, "An analytic solution for the torque between two magnetic dipoles," *Magnetic and Electrical Separation*, Vol. 10, No. 1, 1999, pp. 29-33
- ²⁴Gersh, J. and M. Peck, "Architecting the very-large-aperture flux-pinned space telescope: a scaleable, modular optical array with high agility and passively stable orbital dynamics," *AIAA Guidance, Navigation, and Control Conference*, AIAA, Honolulu, HI, 18-21 Aug. 2008. (in preparation)
- ²⁵Cash, W., "MAXIM preliminary design," proposal to NASA, 2000, URL: <http://maxim.gsfc.nasa.gov/docs/mission/niacdesign.pdf> [cited 30 January 2008]
- ²⁶Meinel, A. B, and M. P. Meinel, "Large sparse-aperture space optical systems", *Optical Engineering*, Vol. 41, No. 8, 2002, pp. 1983-1994.
- ²⁷Zanon, D. J. and M. E. Campbell, "Optimal planner for spacecraft formations in elliptical orbits," *Journal of Guidance, Control, and Dynamics*, Vol. 29, No. 1, Jan-Feb 2006 pp. 161-171.
- ²⁸Campbell, M.E. and B. Udrea, "Collision avoidance in satellite clusters," *Proceedings of the American Control Conference*, Anchorage, AK May 8-10, 2002 pp. 1686-1692. Chen, H. and F. Allgöwer, "A quasi-infinite horizon nonlinear model predictive control scheme with guaranteed stability", *Automatica*, Vol. 34., No. 10, pp. 1205-1217.
- ²⁹Mayne, D. Q. and H. Michalska, "Receding horizon control of nonlinear systems", *IEEE Transactions on Automatic Control*, Vol. 35, No. 7, 1990, pp. 814-824.
- ³⁰Scockaert, P. O. M., J. B. Rawlings, and E. S. Meadows, "Discrete-time stability with perturbations: application to model predictive control", *Automatica*, Vol. 33, No. 3, 1997, pp. 463-470.
- ³¹Sun, J., I. V. Kolmanovskiy, R. Ghaemi, and S. Chen, "A stable block model predictive control with variable implementation horizon", *Automatica*, Vol. 43, No. 11, 2007, pp. 1945-1953.
- ³²L. Breger and J. P. How, "Formation flying control for the MMS mission using GVE-based MPC", *Proceedings of 2005 Conference on Control Applications*, 2005, pp. 565-570.
- ³³Hegrenæs, Ø, J. T. Gravdahl, and P. Tøndel, "Spacecraft attitude control using explicit model predictive control", *Automatica*, Vol. 41, No. 12, 2005, pp. 2107-2114.
- ³⁴Manikonda, V., P. O. Arambel, M. Gopinathan, R. K. Mehra, and F. Y. Hadaegh, "A model predictive control-based approach for spacecraft formation keeping and attitude control", *Proceedings of the 1999 American Control Conference*, 1999, Vol. 5, pp. 4258-4262.
- ³⁵Mehra, R. K., S. Seereeram, J. T. Wen, and D. S. Bayard, "Nonlinear predictive control for spacecraft trajectory guidance, navigation, and control", *Space Technology and Applications International Forum*, edited by Mohamed S. El-Genk, The American Institute of Physics, 1998, pp. 147-152.
- ³⁶Wen, J. T., S. Seereeram, and D. S. Bayard, "Nonlinear predictive control applied to spacecraft attitude control", *Proceedings of the 1997 American Control Conference*, Vol. 3, 1997, pp. 1899-1903.
- ³⁷Wood, M. and W. H. Chen, "Regulation of magnetically actuated satellites using model predictive control with disturbance modeling", *IEEE International Conference on Networking, Sensing and Control*, 2008, pp. 692-697.
- ³⁸Wood, M. and W. H. Chen, and D. Fertin, "Model predictive control of low earth orbiting spacecraft with magnetotorsors", *IEEE International Conference on Control Applications*, 2006, pp. 2908-2913.
- ³⁹Jones, L. and M. Peck "Fractionated solar sails: an analysis of discrete-particle solar sail designs," *AIAA/AAS Astrodynamics Specialist Conference*, AIAA/AAS, Honolulu, HI, 18-21 Aug. 2008. (in preparation)